RESEARCH ARTICLE | MAY 07 2025

Energy distributions of lepton pairs in ultra-intense laser and electrons collision

Ming Zi ; Yan-Yun Ma ; Xiao-Hu Yang ; Guo-Bo Zhang ; Jian-Xun Liu ; Fu-Qiu Shao

Phys. Plasmas 32, 053302 (2025)
https://doi.org/10.1063/5.0254515

Energy distributions of lepton pairs in ultra-intense laser and electrons collision

Cite as: Phys. Plasmas **32**, 053302 (2025); doi: 10.1063/5.0254515
Submitted: 23 December 2024 · Accepted: 18 March 2025 ·
Published Online: 7 May 2025

View Online Export Citation CrossMark

Ming Zi,[1,a)] Yan-Yun Ma,[2,b),c)] Xiao-Hu Yang,[1] Guo-Bo Zhang,[1] Jian-Xun Liu,[3] and Fu-Qiu Shao[1]

AFFILIATIONS

[1]College of Science, National University of Defense Technology, Changsha 410073, China
[2]College of Advanced Interdisciplinary Studies, National University of Defense Technology, Changsha 410073, China
[3]Early Warning Academy, Wuhan 430019, China

[a)]**Electronic mail:** zimingsh@sina.com
[b)]**Author to whom correspondence should be addressed:** yanyunma@126.com
[c)]**Present address:** School of Automation and Electronic Information, Xiangtan University, Hunan 411105, China and School of Physics and Electronics, Hunan University, Changsha 410082, People's Republic of China

ABSTRACT

The energy distribution of positrons was investigated during the interaction of ultra-relativistic electrons with a petawatt-scale laser pulse. This study aims to elucidate the fundamental physics of lepton pair production by examining the interplay between two key mechanisms in the laser field: nonlinear Compton scattering and the nonlinear Breit-Wheeler process. Critical parameters, including laser intensity, electron energy, and collision geometry, were systematically analyzed to uncover the underlying principles governing positron production. The results demonstrate that the positron energy distribution is strongly influenced by the initial electron energy and the collision angle. The energy spectrum of positrons in the head-on collision scenario ($\theta = \pi$) is an order of magnitude higher than that observed in small-angle collision ($\theta = 4\pi/5$). This significantly shapes its spectral characteristics. Furthermore, the observed spectra reveal distinct electron dynamics and cascade effects, providing insights into the complex behavior of particles in ultra-high electromagnetic fields. These findings offer valuable guidance for optimizing experimental setups to enhance positron production efficiency, with potential applications in advanced high-field physics research.

I. INTRODUCTION

With the advancement of Chirped Pulse Amplification (CPA) technology and Optical Parametric CPA (OPCPA), laser power has reached the multi-PW level,[1–3] enabling intensities of up to 10^{23} W/cm^2 in state-of-the-art laser facilities. At such extreme level intensities, quantum electrodynamics (QED) effects dominate the interaction between charged particles and the laser electromagnetic field,[4,5] opening new avenues for scientific exploration in plasma physics, astrophysics, and materials science.[6–8] The electric field in polarization vacuum for electron-positron pair creation is required at the Schwinger field E_s (1.32×10^{18} V/m).[9] Strong field methods utilize the nuclear Coulomb field of high-Z atoms as an alternative for producing positrons. One such method involves colliding an electron beam with a solid target, resulting in the Bethe-Heitler (BH) process and the Trident process.[10,11] The primary process predicted in the fourth-generation synchrotron radiation facility, such as x-ray free-electron lasers (x-ray FEL),[12,13] is the linearly Breit-Wheeler process $\gamma + \gamma' \to e^+ + e^-$.[14] In the regime of ultra-intense, ultra-short laser pulses, the laser itself acts as a target, enabling the spontaneous generation of lepton pairs (electrons and positrons) through the nonlinear Breit-Wheeler (nlBW) process $\gamma + n\omega \to e^+ + e^-$. Here, high-energy photons are produced via nonlinear Compton scattering (nlC) $e^{+,-} + n\omega \to e^{+,-} + \gamma$.[15] The nlBW process has been intensively studied in recent years.[8,16–18] The observation and confirmation of nlBW positrons were achieved using the E144 equipment at Stanford Linear Accelerator Center (SLAC).[19] In this experiment, a laser pulse with an intensity of 10^{18} W/cm^2 and a colliding electron beam with an energy up to 46 GeV from the linear accelerator was utilized.[19] The laser field provides a strong electromagnetic environment. Zhu *et al.* proposed a scheme in which a high-energy electron beam is focused by a conical target and then collides with a solid target to generate polarized positrons.[20] Additionally, laser-plasma wakefield acceleration can produce high-charge electron beams. These electron beams scatter

with counter-propagating laser pulses, generating high-brightness x-ray pulses.[21] An experimental strategy is developed for studying electron-positron pair production at Multi-PW laser facilities.[22] Furthermore, Yuan *et al.* have simulated the interaction of an ultra-intense laser with aluminum (Al) targets of varying transverse sizes.[23] To calculate pair production probabilities, approximation methods such as the local constant field approximation (LCFA) are widely employed in both analytical and numerical studies.[24–27] These methods facilitate the exploration of strong-field QED effects and provide insights into relativistic quantum plasmas and extreme-condition physics.[28,29] Despite significant progress, research on the energy distribution of lepton pairs in laser-electron collisions remains in its early stages, with numerous theoretical and practical challenges yet to be addressed.

The paper is structured as follows. Section II reviews the theoretical framework, including the differential emission rates for nlC and nlBW processes under LCFA, as well as the emission probabilities and optical depths of photons and positrons. Section III investigates the energy distribution of positrons produced in collisions between ultra-relativistic electron beams and ultra-intense laser pulses, comparing our model results with numerical simulations. Finally, Sec. IV summarizes the findings and presents conclusions.

II. NLC PROGRESS AND NLBW PROGRESS

To investigate the details of nonlinear Compton scattering (nlC) and the nonlinear Breit-Wheeler (nlBW) process, we consider the interaction of a relativistic electron with a laser field. Throughout this paper, we employ natural units ($\hbar = c = 1$). and the fine-structure constant is defined as $\alpha_f = e^2/4\pi \approx 1/137$. In momentum representation, the wave function of relativistic electrons and positrons follows the Dirac equation,[30,31]

$$\left(\gamma^\mu p_\mu - e\gamma^\mu A_\mu - m\right)\psi_{p,r}(x) = 0, \tag{1}$$

where $\psi_{p,r}(x)$ is the four-component electron bi-spinor. The vector potential of the laser $A_\mu(\phi)$, with invariant phase $\phi = \kappa \cdot x = k^\mu x_\mu$, here $\kappa = (\omega, \boldsymbol{k})_\mu$, $\boldsymbol{k}$ is the wave vector determines the propagation direction of the laser field. The Volkov solution corresponding to Dirac equation in plane field takes the following form.[30,32] The action parameter S represents the classical Hamilton-Jacobi function of an electron moving in an arbitrary electromagnetic field $A^\mu(\phi)$. The definition of S indicates that the electron's motion in the laser field was treated as classical trajectory.

The probability of gamma photon and pairs production in electromagnetic field is determined by two Lorentz-invariant parameters:[33] $\eta = (e/m_e^3)\left|F_{\mu\nu}p^\nu\right|$ and $\chi = (e/m_e^3)\left|F_{\mu\nu}k^\nu\right|$. $F_{\mu\nu} = \partial_\mu A_\nu - \partial_\nu A_\mu$ is the electromagnetic field tensor. For $\alpha_f \eta^{2/3} \ll 1$ condition, when the electron undergoes a single nonlinear Compton scattering, the transition matrix element takes the lowest order, meaning that the semi-perturbative expansion of strong-field QED is applicable.[32] In this process, an electron collision with external electromagnetic field from an initial state $\psi_p(x)$ to a final state $\psi_{p'}(x)$ in unity volume. In Furry presentation, the laser photons are treated as classical pulse, while the high-frequency γ photons and high-energy leptons are quantized[34] and "dressed" by the low-frequency laser photons. The laser photons are treated as the external field, and the transition amplitude M_{nlCS} of nonlinear Compton scattering at the leading order is given by Di Piazza *et al.* and Ritus.[30,31] In a normalized volume, the number of photon emitted is given by Ritus,[31]

$$dN_{nlC} = N_e \frac{d^3k}{2(2\pi)^2}\frac{d^3p}{(2\pi)^2}\sum_{l,r,r'}(M_{nlC})^2, \tag{2}$$

where N_e is the number of the seed electrons in the laser electromagnetic field.

when the formation length (l_f) of gamma photon and lepton pairs is much shorter than the scale on which the external laser field changes, the field can be considered locally constant.[35] The electron experiences a constant field, which can set as $A^\mu(\phi) = a^\mu\phi$, $a^\mu = (0, \boldsymbol{a})$, is the four-potential vector. Hence, only the instantaneous momentum p^μ is necessary to perform the calculation. To evaluate the photon and pairs spectra, the local values η and χ are used at each particle time step. In the electron's rest frame, the laser field can still be treated as a crossed electromagnetic field. This process is derived from local calculations within the laser pulse envelope over short timescales and is assumed to be adiabatic. Under the LCFA, the local classical kinetic momentum π^μ is a covariant form of momentum and is used as a the replacement for the asymptotic momentum p, which is given by Ritus,[31]

$$\pi^\mu = p^\mu - eA^\mu + k^\mu\left(2eA\cdot p - e^2A\cdot A\right)/(2k\cdot p). \tag{3}$$

Using the relation of Airy function with the asymptotic expression of the Bessel function for the approximation $\mathrm{Ai}(y) = 1/\pi\sqrt{y/3}K_{1/3}\left(\frac{2y^{3/2}}{3}\right)$, the local differential radiation rate probability for an electron to emit one-photon in nonlinear Compton scattering is given by Refs. 31, 36, and 37,

$$\frac{d^2N_{nlCS}}{dtd\omega} = \frac{\alpha_f}{\sqrt{3}\pi\tau_c\gamma_e^2}\left\{\left(2+\frac{3}{2}\chi\delta\right)K_{2/3}(\delta) - \int_\delta^\infty K_{1/3}(s)ds\right\}, \tag{4}$$

here $\delta = \frac{2\chi}{3\eta(\eta-\chi)}$, $\tau_c = 1/m$ is the Compton wavelength, $K_\nu(x)$ is the modified Bessel function of the second kind. Define $\tau_{nlC} = \int\frac{d^2N_{nlC}}{dtd\omega}d\omega$, the probability rate of Compton photon emission per unit time.

For a linearly polarization laser with an intensity $I = 2.3 \times 10^{21}$ W/cm^2, the corresponding electron energy $\gamma_e m$ ranging from 100 times the electron rest mass to 10 000 times the rest mass (from 51.1 MeV to 51.1 GeV). Such an intensity is quite high and is typically achieved using multi-petawatt (PW) lasers systems. The electron energy and laser field satisfy the condition $\alpha\eta^{2/3} \ll 1$, where the process located in the regime of perturbative.[38] The Lorenz invariant η, representing the electric intensity in the electron's rest frame, is expressed as

$$\eta = (1-\cos(\theta))\gamma_e\frac{a_l}{a_s}, \tag{5}$$

where the strength parameter of the laser $a_l = e\sqrt{2I_{lp}/(c\varepsilon_0)}/(m\omega_0 c)$ $f(\phi)$, a_s corresponding to Schwinger strength parameter. θ is the angle shown in Fig. 1 between the direction of electronic motion and the direction of the laser wave vector. As Fig. 2 illustrated, the differential emission rate $d^2N_{nlC}/dtd\omega$ and the emission spectrum $\omega d^2N_{nlC}/dtd\omega$ (normalized by the $\alpha_f/\sqrt{3}\pi\tau_c\alpha_f/\sqrt{3}\pi\tau_c$) in the head-on collision model.

According to the definition of the Lorenz invariant, it derives the relationship of $\eta/\chi = \gamma_e m/\omega$. For $\gamma_e = 100(\eta \sim 0.02)$, at this stage entering to the quantum regime, the emission probability decreases as the photon energy grows. It is indicated that the photons energy

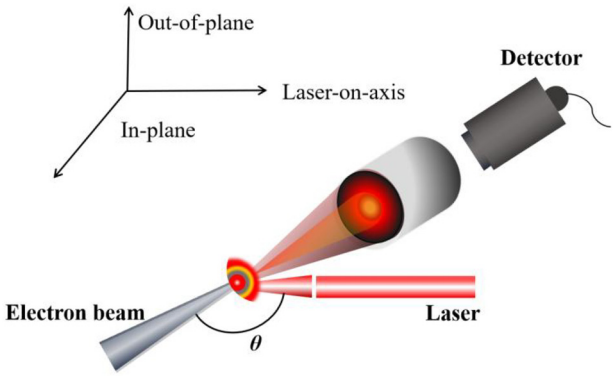

FIG. 1. Schematic diagram of pair production in a laser-electron beam collision. The laser pulse and electron beam collide at a focal point, where nIC and nIBW processes occur. The colors in the collision zone represent the generation of high-energy photons (dark red) and lepton pairs, including positrons (yellow) and electrons (green).

becomes much smaller than that of electron $\omega \ll \gamma_e$. When the electron energy reaches a point at $\gamma_e = 1000$, the photon cutoff energy surpass $0.5\,\gamma_e m$. This signifies that at this stage, photons are more likely to be produced in this energy range, and entering to the QED regime ($\eta \sim 0.2$). The photon spectrum broadens with increasing electron energy. For the electron energy reaches $\gamma_e = 100\,000$, the emission probability peaks near $\omega/\gamma_e m \sim 1$, suggesting a higher likelihood of producing high-energy photons. However, at this line, the emission probability at low energy region decreased compared to $\gamma_e = 10\,000$ scenario. Yet, the emission spectrum is higher on the right panel in Fig. 2, indicating that although the low-energy photon emission probability drops, more electron energy is being converted into high-energy photons, resulting in photon with higher energy. This behavior suggests the onset of photon recoil effects and potential radiation reaction "quenching," where the electron's energy is entirely converted into photons. The peak structure implies a higher probability of producing high-energy ($\omega \sim \gamma_e m$) or even monochromatic photons.[31]

In the quantum regime, high-energy photons can interact with multiple laser photons, leading to electron-positron pair production. As described in Eq. (4), the production of positrons in a normalized volume is given by $dN_{nlBW} = N_\gamma \frac{d^3k}{2(2\pi)^2}\frac{d^3p}{(2\pi)^2}\sum_{l,r,r'}(M_{nlBW})^2$. However, there is an energy threshold for pair production. Only photons with energy greater than twice the electron rest energy m_e can interact with the laser field and lead to pair production. When a high-energy photon decays into lepton pairs (e^+e^-), the differential rate probability is given by Refs. 31 and 39–41,

$$\frac{d^2N_{nlBW}}{dtd\gamma_p} = \frac{\alpha_f m^3}{\sqrt{3}\pi\omega^2}\left\{\left(\frac{3}{2}\chi\rho - 2\right)K_{2/3}(\rho) - \int_\rho^\infty K_{1/3}(s)ds\right\}, \quad (6)$$

where $\rho = \frac{2\chi}{3\eta_p(\chi-\eta_p)}$, and η_p and γ_p refer to the Lorenz invariant and Lorenz factor of the positron created in nlBW process, respectively. In the furry picture, the nlC and nlBW processes are related by crossing symmetry, which is confirmed from the formula above.

As shown in Fig. 3, the colliding laser intensity is fixed at $I = 2.3 \times 10^{21}\,\mathrm{W/cm^2}$. The differential emission rate probability $d^2N_{nlBW}/dtd\gamma_p$ and power spectrum $d^2P_{nlBW}/dtd\gamma_p$ (normalized by the $\alpha_f m_e^3/\sqrt{3}\pi\tau_c$) at different values of electrons energy in Fig. 3. It displays a symmetric distribution structure, when the photon energy is $\omega = 500\,\mathrm{m}$, the emission rate reaches the maximum at a positron energy of $\gamma_p = 250$ and then decreases. As the energy photon increases, a platform structure emerges, which becomes broader as show in Fig. 3, indicating that the produced positron have a broader energy range. This trend differs from that observed in Fig. 2. Remarkably, when photon energy at $\omega = 5000\,\mathrm{m}$, the positron energy spans the entire photon energy range with nearly uniform production probability, contrasting with the nlC emission behavior in Fig. 2. These results have implications for pair creation probability rates at $\chi < 10$, which can be approximated as $dN_{nlBW}/dt \approx 3\pi\alpha m\chi e^{-8/3\chi}/50\omega$.[36,42]

III. SIMULATION OF PAIR PRODUCTION

In the regime of photon emission, the radiation is directed forward into a cone with an opening angle $\sim 1/\gamma_e$, allowing the

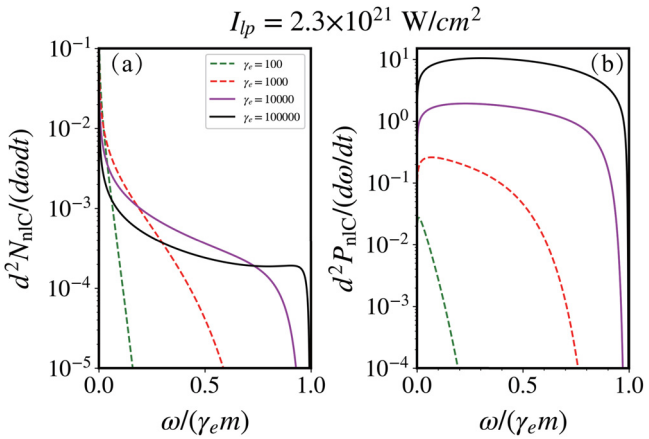

FIG. 2. The photon emission probability (a) and radiation power spectrum (b) as a function of photon energy ω, which is normalized by electron energy $\gamma_e m$. The intensity is fixed to $2.3 \times 10^{21}\,\mathrm{W/cm^2}$ for the laser pulse.

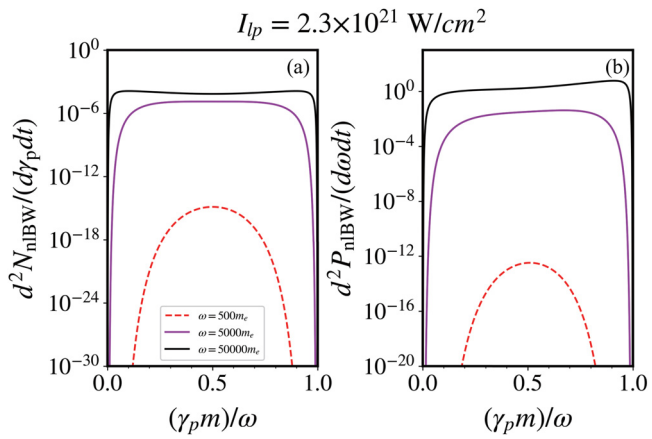

FIG. 3. Positron production rate $d^2N_{nlBW}/dtd\gamma_p$ (a) and power spectrum (b) as a function of positron energy $\gamma_p m$ (scaled by the photon energy ω), with the laser intensity fixed at $2.3 \times 10^{21}\,\mathrm{W/cm^2}$.

momenta of the photon and electron to be treated as collinear. The mean square angle in the quantum limit is given by Blackburn *et al.*[43] $\langle\theta^2\rangle \approx 1.76\gamma^{-2}\eta^{2/3}$. In our model, where $\alpha\eta^{2/3} \ll 1$, we have $\langle\theta^2\rangle \ll 1$, implying that the photon radiation angle is highly collimated around the particle trajectory. For efficient high-energy photon emission, the formation length l_f must be shorter than the characteristic length scale of the laser field. In the context of nonlinear Compton scattering, the formation length of photons emitted by electrons is given by Baier *et al.*,[44]

$$l_f(\omega, \gamma_e, a_0) = \frac{\gamma_e \lambda_c}{\eta}\left(\frac{E_\omega + \eta E_e}{E_\omega}\right)^{1/3}, \tag{7}$$

where $E_\omega = \omega$ and $E_e = \gamma_e m$ are the energy of the photon and electron respectively. Compton wavelength λ_c is approximately equal to 3.86×10^{-13} m. As shown in Fig. 4, the formation length is significantly shorter than the scale of variation of the electromagnetic field ($\sim \lambda_l$). The formation length is different from the formula given in Ref. 45. This observation indicates that the emission process of photons and pairs production may be treated locally, similar in the constant cross field, when the formation length is much smaller than the characteristic length of the external field.

Within the laser field, the quantum modified Landau-Lifshitz (LL) equation governs the motion of electron while considering the effects of radiation reaction. The LL equation decomposed into time and space components, with the canonical relation to the evolution of the energy and momentum of an electron. In our model, the electron $\gamma_e \gg 1$, the evolution of the electron energy and momentum can be described as follows:[46,47]

$$\begin{aligned} m\frac{d\gamma}{dt} &= -e\mathbf{u}\cdot\mathbf{E} - P_r, \\ \frac{d\mathbf{p}}{dt} &= -e(\mathbf{E} + \mathbf{u}\times\mathbf{H}) - P_r\mathbf{u}/\mathbf{u}^2, \end{aligned} \tag{8}$$

where $P_r = 2m\alpha^2\eta^2 g(\eta)/(3\tau_e)$ is defined as the quantum instantaneous power, $g(\eta) = [1 + 4.8(1+\eta)\ln(1+1.7\eta) + 2.44\eta^2]^{-2/3}$ is the quantum correction,[48] which can also be derived from Eq. (4), $\tau_e = e^2/m$, is the momentum of electron. Eq. (8) conserves the on-shell condition, similar to the full LL equation. When considering the electron, in the equation's right-hand side, the electromagnetic contribution can be ignored. This leads to the equation of electron energy in the laser field

$$\frac{d\gamma}{d\phi} = \frac{P_r}{[1 - \cos(\theta)\cos(\varphi)]\omega_0 t}. \tag{9}$$

As we discussed above, we take the laser pulse has a plane form: $a(t,x,y,z) = a_0 \exp[-(x^2+y^2)/r_0^2 - (z+z0)^2/w^2]$. When the laser pulse energy E_l is constant, the peak laser intensity $a_0 \sim E_l/(r_0^{-1}w^{-1/2})$. As depicted in Fig. 1, the laser pulse propagating along z-axis to the left. An ultra-relativistic electron follows a trajectory: $x_e = t\cos(\varphi)\sin(\theta)$, $y_e = t\sin(\varphi)$, $z_e = t\cos(\varphi)\cos(\theta)$, where φ and θ are electron's polar angle and radian angle, respectively. This accounts for the electron's motion within the laser field. The electron in the laser pulse experiences an effective laser intensity,

$$a_{eff}(t, x_e, y_e, z_e) = a_{eff}(\phi) = a_0 \exp\left[-\frac{\phi^2}{4\pi^2 T_{eff}^2}\right], \tag{10}$$

where $T_{eff} = w(1 + \Theta w^2/r_0^2)^{-1/2}/\lambda$ can be treated as the efficient interaction length or time (in nature unit) between electrons and laser pulse, and $\phi = [1 - \cos(\theta)\cos(\varphi)]\omega_0 t$, $\Theta = [\cos(\varphi)\sin(\theta)^2 + \sin(\varphi)^2][1 - \cos(\theta)\cos(\varphi)]^{-2}$. In our configuration (in Fig. 1), the polar angle set to be zero; therefore,

$$T_{eff} = \frac{w}{\lambda}\left\{1 + \frac{w^2}{r_0^2}\tan[(\pi - \theta)/2]^2\right\}^{-1/2}. \tag{11}$$

To quantify the angle dependence of the electron colliding with the laser pulse, Eq. (11) shows the effective wave number, which describes the effective time the electron experiences in the laser field. where $R = w/r_0$ is defined as the radio of the laser pulse width and spot size. As discussed previously, models have shown that there is a trade-off between high laser intensity and the size of the interaction volume. In our model, we set the volume to be constant ($r_0 w^{1/2} = 27\lambda^{3/2}$), and therefore, the peak intensity a_0 is constant. Considering the emission of positrons (photons) is a discontinuous process with the emission rate, and positron (photon) emission events happen in an interval [0, t]. The production of positrons follows the Poisson statistics of parameter τ_{nlBW}:

$$P_n = \frac{\tau_{nlBW}^n}{n!}\exp(-\tau_{nlBW}), \tag{12}$$

where P_n is the probability of producing positron during high-energy photon interaction in the field. The total production number of positrons with the optical depth τ_{nlBW} defined in Eq. (6) is $n_{nlBW} = n_\omega(1 - e^{-\tau_{nlBW}})$, where is the number of photons produced per unit time per electron. The production of positrons and photons is a stochastic process, typically described by its probability distribution at each point in time. In the Poisson statistics, the expected number or average number of positrons produced per unit time is $\langle n\rangle = \sum nP_n = \tau_{nlBW}$. Therefore, the number of positrons produce per unit time can be calculated.[49] As shown in Fig. 4, the formation length is much shorter than the laser pulse, and the nlBW and nlC processes occur in a point-like manner. Thus, we propose an estimation of the energy distribution of produced positrons by electrons colliding with the laser pulse. The nlC photons are produced in the pulse, and then

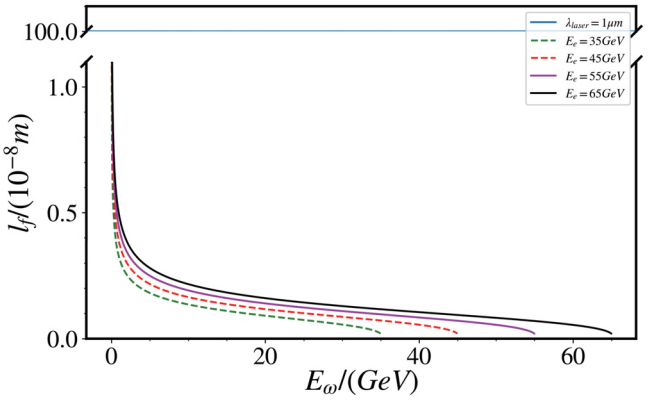

FIG. 4. Formation length of high-energy photons in the head-on collision between electrons and the laser pulse in this simulation.

these photons produce positrons through nlBW. The energy distribution of the positron is given by

$$\frac{dN_p}{d\gamma_p} = \frac{(\pi n_{eff})^2}{2\omega_0^2}\int_{\gamma_p}^{\gamma} d\omega \left[\frac{d^2N_{nlBW}(\gamma,\gamma_p,\omega)}{dtd\gamma_p}\frac{d^2N_{nlC}(\gamma,\omega)}{dtd\omega}\right]. \quad (13)$$

Based on experimental parameters from strong-field QED studies,[50,51] we fix the ratio $R = 8$, corresponding to a relatively long laser pulse width. Moreover, to protect the optical components, the electron beam typically collides with the laser pulse at an angle θ, for example, in LUXE the electron beam colliding to the laser pulse at an angle: $\pi - \theta \approx \pi/10$.[50,51] Taking into account these considerations and the state-of-the-art equipment conditions in Eq. (13), incorporating these considerations, the positron energy spectra are shown in Fig. 5.

As the effective time T_{eff} defined in Eq. (11) decreases with increasing collision angle ($9\pi/10$ to $11\pi/10$), the positron energy spectra shift toward higher energies, as shown in Fig. 5. This shift indicates a higher probability of producing high-energy positrons, which are more likely to trigger cascade processes. The colliding angle from $4\pi/5$ to π reveal the estimation of the characteristic spectra of the positron energy distribution $dN_p/d\gamma_p$, which is obtained via a convolution of nlC process and nlBW process as described in Eq. (13). The structure is push forward to high energies zone, resulting in an increased probability of the positrons having high energy. This character of the positron energy distribution indicates that the produce positrons are more likely to trigger cascade progress. Notably, the peak structure observed at a colliding angle of $\theta = \pi$ is more than an order of magnitude higher than that at $\theta = 4\pi/5$. The plateau structure of the positron energy distribution emerges when the electron energy increases to 100 000 m. Furthermore, a pronounced peak structure near the point $\gamma_p = \gamma_e$, where the colliding electron has energy $\gamma_e = 10\,000$. The methodology employed in this paper differs from that in some previous studies,[43,52] as we employ an analytical approach to analyze the laser-electron collision geometry, contrasting with Blackburn's analytical results.

In Fig. 6(a), which reveals that while PIC simulations exhibit an increasing trend in the high-energy region, they lack the plateau

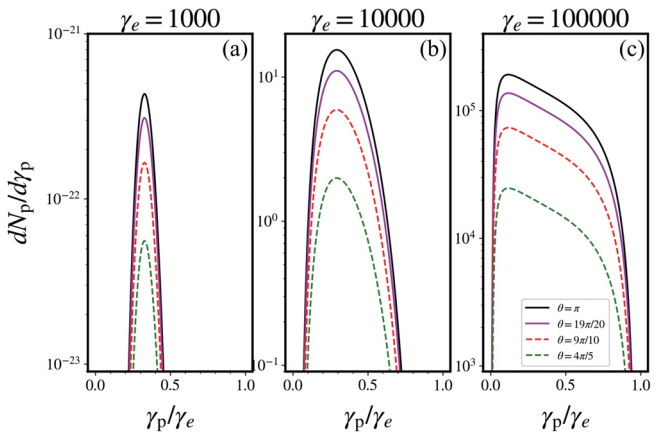

FIG. 5. Positron energy distribution $dN_p/d\gamma_p$ for $R = 8$, and electron energy $\gamma_e = 1000$ (a), 10 000 (b), 100 000 (c), at a different colliding angle of $\theta = \pi$ (black), $19\pi/20$ (red), $9\pi/10$ (red dashed), $4\pi/5$ (green dashed).

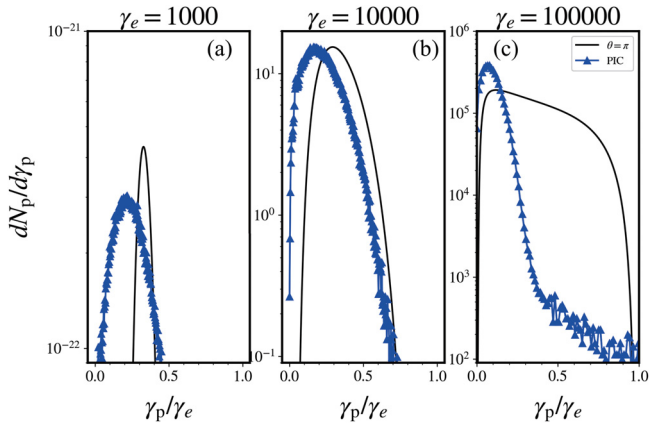

FIG. 6. Comparison of positron energy distribution $dN_p/d\gamma_p$ obtained with Eq. (13) (black line), and from the simulation using PIC code (blue line). The colliding electrons with $\gamma_e = 1000$ (a), $\gamma_e = 10\,000$ (b), and $\gamma_e = 100\,000$ (c).

structure observed in our model. Notably, for electron Lorentz factors of $\gamma_e = 1000$ and $\gamma_e = 10000$, the PIC simulations agree well with our results regarding positron yield. However, the Monte Carlo PIC code employs a random distribution of photon and positron energies in the nlC and nlbBW processes. In contrast, our coupled model is based on the assumption that the formation length is significantly shorter than the characteristic length of the laser field, and the electron Lorentz factor is much larger than the dimensionless laser parameter ($\gamma_e \gg a_0$). This discrepancy may lead to an overestimation of high-energy positrons in our model, particularly in the high-energy zone as shown in Fig. 6(c). The high-energy zone reaching up to 1 is a result of the electron "quenching" effect, where positrons initiate a cascade process, progressively transferring the energy of incident electrons, a phenomenon often referred to as an avalanche cascade. In the low-energy region, the positron energy spectrum from Epoch simulations shows a broader energy characteristic compared to our model. In the medium-energy region, there is a good alignment between the Epoch model and our model. However, the Monte Carlo PIC code employs a random distribution of photon and positron energies in the nlC and nlBW processes. In contrast, our coupled model is based on the assumption that the formation length is significantly shorter than the characteristic length of the laser field, and the electron Lorentz factor is much larger than the dimensionless laser parameter. This discrepancy may lead to an overestimation of high-energy positrons in our model. Our model is better suited for astrophysical simulations, while PIC codes like Epoch are optimized for ultra-intense laser-solid interactions. In conclusion, the Epoch model separates the two processes and uses a particle-based approach, while our model provides a coupled analysis based on density distributions. The choice between these approaches depends on the specific physical context and parameters of the simulation.

IV. SUMMARY

In this paper, we present a comprehensive theoretical model to explore the energy distribution of positrons generated from the interaction between ultra-relativistic electrons and multi-petawatt (PW)-scale laser pulses. By leveraging the Poisson distribution, we provide a

robust framework for understanding the stochastic nature of positron production and its correlation with high-energy photon emission. Our model focuses on the coupled processes of nonlinear Compton scattering and nonlinear Breit-Wheeler pair production, which are central to the generation of positrons in high-intensity laser-electron collisions. Through detailed analysis, we elucidate the interplay between these processes and their impact on the energy spectra of positrons, offering new insights into the underlying physical mechanisms.

The interaction between ultra-relativistic electrons and intense laser fields is governed by strong-field quantum electrodynamics (QED) effects, where the formation length of photons and positrons is significantly shorter than the characteristic scale of the laser field. This allows us to treat the emission processes locally, akin to a constant crossed field approximation. We derive the differential emission rates for both nlC and nlBW processes under the local constant field approximation (LCFA), which is validated by the condition $\alpha\eta^{2/3} \ll 1$. Our results reveal that the energy distribution of positrons is highly sensitive to the initial electron energy, laser intensity, and collision geometry. Specifically, we observe that higher electron energies and optimal collision angles enhance the production of high-energy positrons, which are crucial for triggering cascade processes in strong-field QED. One of the key findings of our study is the emergence of distinct spectral features in the positron energy distribution, including characteristic structures and pronounced peaks near the maximum energy limit ($\gamma_p = \gamma_e$). These features are indicative of the photon recoil effect and the onset of radiation reaction "quenching," where the electron's energy is entirely converted into high-energy photons and positrons.

In conclusion, our theoretical model provides a detailed and versatile framework for analyzing the energy distribution of positrons in ultra-intense laser-electron collisions. By coupling the nlC and nlBW processes and incorporating stochastic effects through Poisson statistics, we offer a deeper understanding of the complex dynamics involved in positron production. Our findings not only advance the theoretical understanding of strong-field QED but also pave the way for innovative experimental designs and applications in various scientific and technological fields. Future work will focus on refining the model to include multi-photon effects and exploring its applicability to astrophysical environments, where similar processes may occur under extreme conditions.

ACKNOWLEDGMENTS

This work was supported by the National Natural Science Foundation of China (Grant Nos. 12175309, 12475252, and 12275356). The authors wish to acknowledge CFSA at University of Warwick for allowing usage of EPOCH.

AUTHOR DECLARATIONS

Conflict of Interest

The authors have no conflicts to disclose.

Author Contributions

Ming Zi: Investigation (equal); Writing – original draft (equal). **Yan-Yun Ma:** Investigation (equal); Supervision (equal). **Xiao-Hu Yang:** Resources (lead); Supervision (equal). **Guo-Bo Zhang:** Methodology (equal); Resources (equal). **Jian-Xun Liu:** Investigation (equal); Methodology (equal). **Fu-Qiu Shao:** Investigation (equal); Supervision (equal).

DATA AVAILABILITY

The data that support the findings of this study are available from the corresponding author upon reasonable request.

REFERENCES

[1]V. Yakimenko, L. Alsberg, E. Bong, G. Bouchard, C. Clarke, C. Emma, S. Green, C. Hast, M. J. Hogan, J. Seabury, N. Lipkowitz, B. O'Shea, D. Storey, G. White, and G. Yocky, "FACET-II facility for advanced accelerator experimental tests," Phys. Rev. Accel. Beams **22**, 101301 (2019).
[2]A. M. Fedotov, N. B. Narozhny, G. Mourou, and G. Korn, "Limitations on the attainable intensity of high power lasers," Phys. Rev. Lett. **105**, 080402 (2010).
[3]C. Jiang, Z. Zhang, H. Dong, Z. Shi, J. He, S. Hao, F. Sun, J. Gui, J. Qian, and J. Zhu, "Generation and application of high-contrast laser pulses using plasma mirror in the SULF-1PW beamline," Chin. Opt. Lett. **21**, 043802 (2023).
[4]V. I. Sokolov, M. N. Naumova, and A. J. Nees, "Numerical modeling of radiation-dominated and quantum-electrodynamically strong regimes of laser-plasma interaction," Phys. Plasmas **18**, 093109 (2011).
[5]C. N. Harvey, A. Gonoskov, A. Ilderton, and M. Marklund, "Quantum quenching of radiation losses in short laser pulses," Phys. Rev. Lett. **118**, 105004 (2017).
[6]P. Sprangle, B. Hafizi, A. Ting, and R. Fischer, "High-power lasers for directed-energy applications," Appl. Opt. **54**, F201 (2015).
[7]A. Y. Chen, Y. Yuan, and H. Yang, "Physics of pair producing gaps in black hole magnetospheres," Astrophysical J. **863**, L31 (2018).
[8]N. B. Narozhny, S. S. Bulanov, V. D. Mur, and V. S. Popov, "On e^+e^- pair production by a focused laser pulse in vacuum," Phys. Lett. A **330**, 1–6 (2004).
[9]S. S. Bulanov, T. Z. Esirkepov, A. G. Thomas, J. K. Koga, and S. V. Bulanov, "Schwinger limit attainability with extreme power lasers," Phys. Rev. Lett. **105**, 220407 (2010).
[10]G. Sarri, K. Poder, J. M. Cole, W. Schumaker, A. Di Piazza, B. Reville, T. Dzelzainis, D. Doria, L. A. Gizzi, and G. Grittani, "Generation of neutral and high-density electron–positron pair plasmas in the laboratory," Nat. Commun. **6**, 6747 (2015).
[11]S. V. Bulanov, T. Z. Esirkepov, M. Kando, J. Koga, K. Kondo, and G. Korn, "On the problems of relativistic laboratory astrophysics and fundamental physics with super powerful lasers," Plasma Phys. Rep. **41**, 1–51 (2015).
[12]C. Feng and H. X. Deng, "Review of fully coherent free-electron lasers," Nucl. Sci. Tech. **29**, 3–17 (2018).
[13]H.-S. Kang, C.-K. Min, H. Heo, C. Kim, H. Yang, G. Kim, I. Nam, S. Y. Baek, H.-J. Choi, G. Mun *et al.*, "Hard x-ray free-electron laser with femtosecond-scale timing jitter," Nat. Photonics **11**, 708–713 (2017).
[14]O. J. Pike, F. Mackenroth, E. G. Hill, and S. J. Rose, "A photon–photon collider in a vacuum hohlraum," Nat. Photonics **8**, 434–436 (2014).
[15]Q. Z. Lv, E. Raicher, C. H. Keitel, and K. Z. Hatsagortsyan, "High-brilliance ultranarrow-band x rays via electron radiation in colliding laser pulses," Phys. Rev. Lett. **128**, 024801 (2022).
[16]H. M. Thoma, "*Colloquium:* Field theoretic description of ultrarelativistic electron-positron plasmas," Rev. Mod. Phys. **81**, 959–968 (2009).
[17]C. Ridgers, C. S. Brady, R. Duclous, J. Kirk, K. Bennett, T. Arber, A. Robinson, and A. Bell, "Dense electron-positron plasmas and ultraintense γ rays from laser-irradiated solids," Phys. Rev. Lett. **108**, 165006 (2012).
[18]M. G. Lobok, A. V. Brantov, and V. Yu. Bychenkov, "Effective production of gammas, positrons, and photonuclear particles from optimized electron acceleration by short laser pulses in low-density targets," Phys. Plasmas **26**, 123107 (2019).
[19]C. Bula, K. McDonald, E. Prebys, C. Bamber, S. Boege, T. Kotseroglou, A. Melissinos, D. Meyerhofer, W. Ragg, D. Burke *et al.*, "Observation of nonlinear effects in Compton scattering," Phys. Rev. Lett. **76**, 3116 (1996).
[20]X.-L. Zhu, W.-Y. Liu, T.-P. Yu, M. Chen, S.-M. Weng, W.-M. Wang, and Z.-M. Sheng, "Dense polarized positrons from beam-solid interaction," Phys. Rev. Lett. **132**, 235001 (2024).

[21]L. Han, J. Cai, Y. Shou, X. Liu, J. Yu, and X. Yan, "Linear Breit-Wheeler process driven by compact lasers," Phys. Rev. E **108**, 055208 (2023).
[22]W. Luo, Y.-B. Zhu, H.-B. Zhuo, Y.-Y. Ma, Y.-M. Song, Z.-C. Zhu, X.-D. Wang, X.-H. Li, I. Turcu, and M. Chen, "Dense electron-positron plasmas and gamma-ray bursts generation by counter-propagating quantum electrodynamics-strong laser interaction with solid targets," Phys. Plasmas **22**, 063112 (2015).
[23]T. Yuan, M. Chen, J. Y. Yu, W. Y. Liu, W. Luo, S. M. Weng, and Z. M. Sheng, "Target transverse size and laser polarization effects on pair production during ultra-relativistic-intense laser interaction with solid targets," Phys. Plasmas **24**, 063104 (2017).
[24]A. Di Piazza, M. Tamburini, S. Meuren, and C. H. Keitel, "Improved local-constant-field approximation for strong-field QED codes," Phys. Rev. A **99**, 022125 (2019).
[25]Q. Lv, E. Raicher, C. Keitel, and K. Hatsagortsyan, "Anomalous violation of the local constant field approximation in colliding laser beams," Phys. Rev. Res. **3**, 013214 (2021).
[26]D. Seipt and B. King, "Spin-and polarization-dependent locally-constant-field-approximation rates for nonlinear Compton and Breit-Wheeler processes," Phys. Rev. A **102**, 052805 (2020).
[27]F. Wan, Y. Wang, R.-T. Guo, Y.-Y. Chen, R. Shaisultanov, Z.-F. Xu, K. Z. Hatsagortsyan, C. H. Keitel, and J.-X. Li, "High-energy γ-photon polarization in nonlinear Breit-Wheeler pair production and γ polarimetry," Phys. Rev. Res. **2**, 032049 (2020).
[28]Y. Shi, H. Qin, and N. J. Fisch, "Plasma physics in strong-field regimes: Theories and simulations," Phys. Plasmas **28**, 042104 (2021).
[29]I. V. Sokolov, N. M. Naumova, J. A. Nees, and G. A. Mourou, "Pair creation in QED-strong pulsed laser fields interacting with electron beams," Phys. Rev. Lett. **105**, 195005 (2010).
[30]A. Di Piazza, C. Müller, K. Z. Hatsagortsyan, and C. H. Keitel, "Extremely high-intensity laser interactions with fundamental quantum systems," Rev. Mod. Phys. **84**, 1177–1228 (2012).
[31]V. Ritus, "Quantum effects of the interaction of elementary particles with an intense electromagnetic field," J. Sov. Laser Res. **6**, 5972043 (1985).
[32]R. Ruffini, G. Vereshchagin, and S.-S. Xue, "Electron–positron pairs in physics and astrophysics: From heavy nuclei to black holes," Phys. Rep. **487**, 1–140 (2010).
[33]S. Bulanov, C. Schroeder, E. Esarey, and W. Leemans, "Electromagnetic cascade in high-energy electron, positron, and photon interactions with intense laser pulses," Phys. Rev. A **87**, 062110 (2013).
[34]W. Furry, "On bound states and scattering in positron theory," Phys. Rev. **81**, 115 (1951).
[35]T. Blackburn, "Measuring quantum radiation reaction in laser electron-beam collisions," Plasma Phys. Controlled Fusion **57**, 075012 (2015).
[36]T. Blackburn, A. Ilderton, C. Murphy, and M. Marklund, "Scaling laws for positron production in laser-electron-beam collisions," Phys. Rev. A **96**, 022128 (2017).
[37]B. King, "Interference effects in nonlinear Compton scattering due to pulse envelope," Phys. Rev. D **103**, 036018 (2021).
[38]P. Zhang, S. S. Bulanov, D. Seipt, A. V. Arefiev, and A. G. R. Thomas, "Relativistic plasma physics in supercritical fields," Phys. Plasmas **27**, 050601 (2020).
[39]T. Blackburn and M. Marklund, "Nonlinear Breit–Wheeler pair creation with bremsstrahlung γ rays," Plasma Phys. Controlled Fusion **60**, 054009 (2018).
[40]A. Golub, S. Villalba-Chávez, H. Ruhl, and C. Müller, "Linear Breit-Wheeler pair production by high-energy bremsstrahlung photons colliding with an intense x-ray laser pulse," Phys. Rev. D **103**, 016009 (2021).
[41]M. Jansen, J. Kamiński, K. Krajewska, and C. Müller, "Strong-field Breit-Wheeler pair production in short laser pulses: Relevance of spin effects," Phys. Rev. D **94**, 013010 (2016).
[42]T. Grismayer, M. Vranic, J. L. Martins, R. Fonseca, and L. O. Silva, "Seeded QED cascades in counterpropagating laser pulses," Phys. Rev. E **95**, 023210 (2017).
[43]T. G. Blackburn, D. Seipt, S. S. Bulanov, and M. Marklund, "Radiation beaming in the quantum regime," Phys. Rev. A **101**, 012505 (2020).
[44]N. V. Baier, M. V. Katkov, and M. V. Strakhovenko, "Quantum radiation theory in inhomogeneous external fields," Nucl. Phys. B **328**, 387–405 (1989).
[45]C. P. Ridgers, J. G. Kirk, R. Duclous, T. G. Blackburn, C. S. Brady, K. Bennett, T. D. Arber, and A. R. Bell, "Modelling gamma-ray photon emission and pair production in high-intensity laser–matter interactions," J. Comput. Phys. **260**, 273–285 (2014).
[46]F. Niel, C. Riconda, F. Amiranoff, R. Duclous, and M. Grech, "From quantum to classical modeling of radiation reaction: A focus on stochasticity effects," Phys. Rev. E **97**, 043209 (2018).
[47]M. Vranic, J. L. Martins, J. Vieira, R. A. Fonseca, and L. O. Silva, "All-optical radiation reaction at 10^{21} W/cm^2," Phys. Rev. Lett. **113**, 134801 (2014).
[48]A. Sokolov, I. Ternov, V. Bagrov, D. Galzov, and V. Shukovskii, "Radiation-induced spin polarization of electrons moving in a spiral orbit in a magnetic field," Tech. Rep. (Moscow State University, 1968).
[49]A. Bell and J. G. Kirk, "Possibility of prolific pair production with high-power lasers," Phys. Rev. Lett. **101**, 200403 (2008).
[50]R. Jacobs, "Luxe: A new experiment to study non-perturbative QED in e^--laser and γ-laser collisions," in SciPost Physics Proceedings 088 (2022).
[51]L. Funcke, T. Hartung, B. Heinemann, K. Jansen, A. Kropf, S. Kühn, F. Meloni, D. Spataro, C. Tüysüz, and Y. C. Yap, "Studying quantum algorithms for particle track reconstruction in the luxe experiment," J. Phys.: Conf. Ser. **2438**, 012127 (2023).
[52]Ó. Amaro and M. Vranic, "Optimal laser focusing for positron production in laser–electron scattering," New J. Phys. **23**, 115001 (2021).